CHEMISTRY OF MATERIALS

Open Access

pubs.acs.org/cm

Article

Robust Co(II)-Based Metal–Organic Framework for the Efficient Uptake and Selective Detection of SO_2

Valeria B. López-Cervantes,[#] Alfredo López-Olvera,[#] Juan L. Obeso,[#] Iván Kaleb Torres, Eva Martínez-Ahumada, Paulina Carmona-Monroy, Elí Sánchez-González, Diego Solís-Ibarra,* Enrique Lima, Elnaz Jangodaz, Ravichandar Babarao, Ilich A. Ibarra,* and Shane G. Telfer*

Cite This: *Chem. Mater.* 2024, 36, 2735–2742

Read Online

ACCESS | Metrics & More | Article Recommendations | Supporting Information

ABSTRACT: MUF-16 is a porous metal–organic framework comprising cobalt(II) ions and 5-aminoisophthalate ligands. Here, we measured its reversible SO_2 adsorption–desorption isotherm around room temperature and up to 1 bar and observed a high capacity for SO_2 (2.2 mmol g^{-1} at 298 K and 1 bar). The uptake of SO_2 was characterized by Fourier transform infrared (FT-IR) spectroscopy, which indicated hydrogen bonding between the SO_2 guest molecules and amino functional groups of the framework. The location and packing of the SO_2 molecules were confirmed by computational studies, namely, density functional theory (DFT) calculations of the strongest adsorption site and grand canonical Monte Carlo (GCMC) simulations of the adsorption isotherm. Furthermore, MUF-16 showed a remarkable selective fluorescence response to SO_2 compared to other gases (CO_2, NO_2, N_2, O_2, CH_4, and water vapor). The possible fluorescence mechanism was determined by using time-resolved photoluminescence. Also, the limit of detection (LOD) was calculated to be 1.26 mM (~80.72 ppm) in a tetrahydrofuran (THF) solution of SO_2.

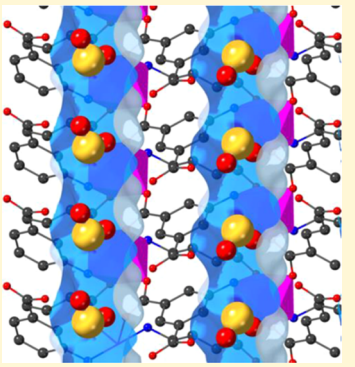

1. INTRODUCTION

An undesirable consequence of the exponential growth of industrial activities is the generation of air pollution, which considerably compromises the air quality of our planet.[1] Reducing air pollution is a priority activity since the constant retention of such contaminant gases in the atmosphere, from different emission sources, leads to negative effects. This relates not only to Earth's temperature, e.g., CO_2 is strongly associated with the greenhouse effect,[2] but also to environmental health as sulfur-containing gases have severely toxic effects on humans.[3] The burning of fossil fuels produces sulfur oxides.[4] The sectors responsible for the largest emission of these polluting gases are the energy and the metallurgical industries.[5] In addition, nonanthropogenic emissions caused by volcanic eruptions constitute approximately 30% of emitted sulfur oxides.[6] When combined with water, which is present in the atmosphere, these compounds can cause acid rain, which causes severe damage to structures and buildings.[7] Additionally, acid rain is responsible for the alteration of the sulfur cycle, causing the adsorption of heavy metals by plants.[8]

Additionally, when humans are exposed to sulfur dioxide (SO_2), it can cause breathing difficulties. At high concentrations, it can produce irreversible intoxication, leading to death.[9] The concentration of SO_2 over periods of 10 min must not exceed about 10 ppm, and the maximum regulated concentration limits to protect health are 0.075 ppm for a 1 h limit. Safety guidelines recommend a maximum concentration in the range of 0.025–0.04 ppm for SO_2 exposure over 24 h.[10]

Thus, many strategies have been developed for SO_2 remediation,[11] such as alkaline solutions for flue gas desulfurization (FGD),[12] ionic liquids (ILs),[13] and classical porous materials such as metal oxides,[14] activated carbons,[15] and zeolites.[16] Unfortunately, these technologies need high reactivation temperatures, which cause a loss of structure stability and, therefore, considerably decrease their capture capacity over multiple cycles.[17] Additionally, in some cases, the chemisorption of SO_2 occurs, which adds to the energy penalty for regeneration.[16]

Metal–organic frameworks (MOFs) are a class of porous materials formed by metal centers and organic linkers such as carboxylates and nitrogen-containing ligands.[18] Certain MOFs have shown high SO_2 capacities at 298 K and 1 bar. For example, MFM-300(M) (M = Al^{3+}, In^{3+}, Sc^{3+}),[19] MIL-101(Cr)-4F(1%),[20] strongly adsorb SO_2. More recently, the uptake capacity of Mg_2(dobpdc) (dobpdc = 4,4′-dioxido-3,3′-biphenyldicarboxylate) was shown to be exceptionally high (19.5 mmol g^{-1}).[21] It is worth noting that high SO_2 uptakes are not the only key consideration in the field of environmental remediation; MOF materials with moderate to low SO_2

Received: October 23, 2023
Revised: February 19, 2024
Accepted: February 21, 2024
Published: March 5, 2024

adsorption provide valuable information, particularly in the context of SO_2 detection.[22]

Small and low-cost SO_2 gas detectors are crucial for the safety of workers who are exposed to various industrial processes. Optical methods including ultraviolet (UV) absorption spectroscopy,[23] mass spectrometry,[24] multiaxis differential optical absorption spectroscopy (MAX-DOAS),[25] and emission (photoluminescence) spectroscopy (PL) have been used in the detection of SO_2, allowing for real-time SO_2 monitoring.[26] A remarkable example of an MOF-based SO_2 detector was elegantly provided by Eddaoudi and co-workers.[27] In the first case using the MOF MFM-300 as a system that selectively detected SO_2 versus CH_4, CO_2, NO_2, and H_2 electrochemically, the device showed a detection limit of 5 ppb and exceptional cyclability.[27] In another case, they reported that KAUST-7 and KAUST-8 materials could be used for the selective capture and detection of SO_2, also electrochemically, reaching detection limits of 25 ppm.[28] Later, Cao and co-workers presented another MOF-based detector, which relied on the photoluminescence response of MOF-5-NH_2 to SO_2.[29] Recently, we have demonstrated selective SO_2 detection by a metal−organic polyhedron (MOP-CDC).[30]

We previously reported the synthesis, characterization, and CO_2 separation by a microporous cobalt-based MOF named MUF-16 (MUF = Massey University Framework).[31] MUF-16 is built up from 5-aminoisophthalate (Haip) linkers and divalent cobalt centers, which adopt an octahedral coordination geometry. Interestingly, MUF-16 adopts a three-dimensional (3-D) lattice, which is supported by hydrogen bonds between carboxyl motifs (Figure 1). Due to the simple, accessible, and scalable synthesis of MUF-16, we decided to investigate the SO_2 adsorption and fluorescence properties of this MOF material. We establish the affinity of MUF-16 for SO_2 and determine its detection capacity by taking advantage of its luminescent properties,[32] which may be employed for the fabrication of SO_2 detectors.

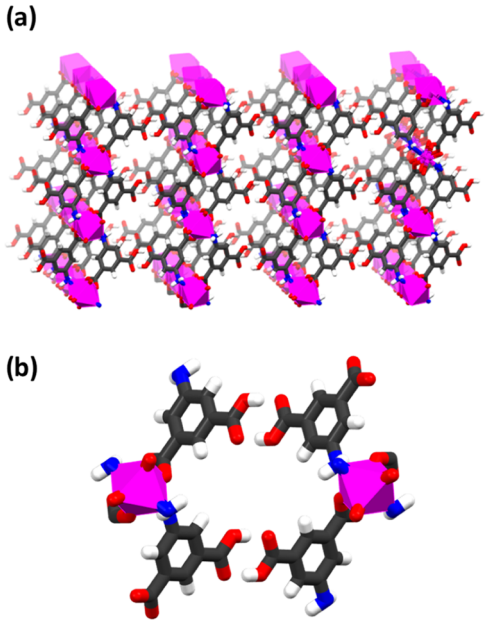

Figure 1. (a) MUF-16 view along the crystallographic *b* axis. (b) Close-up view of the pore channel formed by four H_2aip and two octahedrally coordinated Co(II) centers. Atom labels: carbon = black, nitrogen = blue, oxygen = red, cobalt(II) = pink.

2. EXPERIMENTAL SECTION

2.1. Synthesis of MUF-16. A mixture of $Co(OAc)_2{\cdot}4H_2O$ (0.625 g, 2.5 mmol), 5-aminoisophthalic acid (1.8 g, 10 mmol), methanol (80 mL), and water (5 mL) was sonicated for 25 min in a sealed 1000 mL Schott bottle, which was then heated in a preheated oven at 85 °C for 2 h under autogenous pressure. After cooling the oven to room temperature, the resulting pink crystals were isolated by decanting off the mother liquor, washed with methanol several times, and dried under vacuum at 130 °C for 20 h. Yield: 0.98 g (94% based on cobalt) of guest-free MUF-16.

2.2. Instruments. Further details related to instrumental techniques are presented in Section S1.

2.3. Gas Adsorption Isotherms. The CO_2 and SO_2 adsorption experiments to measure absorbance capacity were performed on the Advantage One Dynamic Vapor Sorption (DVS) equipment of surface measurement systems (SMS). The gravimetric capture of the gases was measured by placing a 23 mg sample of the material in a constant flow of ultrapure grade SO_2 (99.9995%) and CO_2 (99.9%) purchased from INFRA.

2.4. Fluorescence Experiments. Fluorescence spectra were carried out in an Edinburgh Instruments FS5 Spectrofluorometer using a continuous wave 150 W ozone-free xenon arc lamp at room temperature coupled with the SC-10 solid-state sample holder. The samples were packed into quartz sample holders and positioned in the instrument. Emission measurements were carried out using an excitation wavelength of 360 nm with an LP-395 filter on the detector side to remove any remaining light from the excitation source. Emission and excitation measurements were collected with a step size of 1 nm and a dwell time of 0.1 s. The excitation bandwidth was set at 3.00 nm, and the emission bandwidth for the detector was set at 2.00 nm. Time-resolved photoluminescence (TRPL) experiments were measured in an Edinburgh Instruments FS5 Spectrofluorometer using a 375 nm EPL laser, with an excitation bandwidth of 0.01 nm and an emission bandwidth of 2.00 nm at an emission wavelength of 455 nm.

3. RESULTS AND DISCUSSION

3.1. Characterization of MUF-16. The material MUF-16, $[Co(Haip)_2]$, was synthesized via the solvothermal reaction of cobalt acetate ($Co(OAc)_2{\cdot}4H_2O$) and 5-aminoisophthalic acid (H_2aip) in a mixture of MeOH/H_2O/MeCN.[31,33] The resulting pink microcrystals were characterized by powder X-ray diffraction, FT-IR spectroscopy, N_2 adsorption experiments, thermogravimetric analysis, and scanning electron microscopy (SEM) images (Figures S1−S5), corroborating the obtention of the desired crystalline phase; its thermal stability is up to 400 °C and the Brunauer−Emmett−Teller (BET) surface area was 217 $g^2\ m^{-1}$. The average particle size of 3.47 μm was determined with ImageJ software.[34]

3.2. SO_2 Adsorption−Desorption Measurements. Prior to the SO_2 adsorption−desorption studies, the MUF-16 sample was activated at 403 K under a vacuum (1×10^{-3} bar) for 8 h. Figure 2a shows the SO_2 adsorption−desorption isotherm at 298 K and up to 1 bar. Initially, a strong adsorption of 1.40 mmol g^{-1} can be seen in the low-pressure region up to 0.03 bar, which would indicate an affinity of MUF-16 for SO_2. Beyond 0.2 bar, steady plateau adsorption is observed, leading to a saturation capacity of 2.20 mmol g^{-1} at 1 bar. The saturation capacity of MUF-16 is comparable to other MOFs with a similar surface area, for example, KAUST-7 and −8,[28] MIL-53-NO_2,[35] and UNAM-1[36] (Table 1).

The isosteric enthalpy of adsorption for the binding of SO_2 to MUF-16 was calculated from adsorption isotherms at 298 and 308 K employing the virial method at low coverage.[37] It was calculated in the range of −43.7−51.5 kJ mol^{-1} (Figure S6), which corresponds to a strong physisorption process and

https://doi.org/10.1021/acs.chemmater.3c02715
Chem. Mater. 2024, 36, 2735−2742

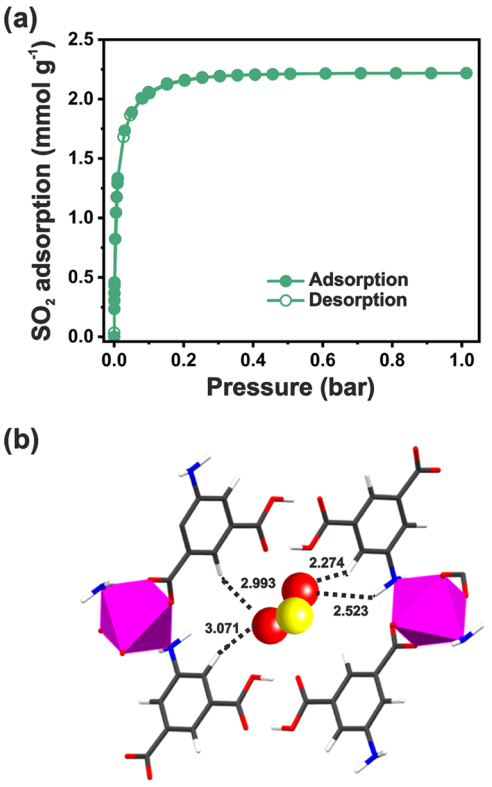

Figure 2. (a) Experimental SO_2 adsorption−desorption isotherm at 298 k and up to 1 bar for activated MUF-16. Filled circles = adsorption; hollow circles = desorption. (b) Main SO_2 adsorption site in MUF-16 identified by DFT-D3 calculation. The interaction distance varies from 2.27 to 3.1 Å, which is assigned to −CH···O═S═O; meanwhile, the 2.52 Å belongs to $-NH_2$···O═S═O. Atom label; carbon: black, nitrogen: blue, oxygen: red, cobalt: pink, and sulfur: yellow.

Table 1. SO_2 Capture in mmol g^{-1}

material	1 bar	0.1 bar	ppm level	refs
MUF-16 (217 m^2 g^{-1})	2.22	2.05	1.33 at 1000 ppm	this work
KAUST-7 (280 m^2 g^{-1})	2.2[a]	-	1.4 at 500 ppm	28
KAUST-8 (258 m^2 g^{-1})	2.2[a]	-	-	
MIL-53-NO_2	3.5	2.07	0.12 at 1000 ppm	35
UNAM-1 (522 m^2 g^{-1})	3.5	1.6	-	36

[a]Measured in the SO_2/N_2:7/93 mixture.

whereby the strong capture at low pressures of SO_2 is justified. This value is comparable with other MOFs with a similar surface area, for example, Co-URJC-5[22] and UNAM-1.[36] Clearly, the adsorption and desorption branches coincide, excluding a possible hysteresis and confirming an SO_2 physisorption process.[36] The structural stability following SO_2 adsorption/desorption was assessed by powder X-ray diffraction (PXRD) (Figure S7) and IR (Figure S8).

The unchanged nature of the PXRD pattern shows that the crystal structure of MUF-16 was retained, which is consistent with the reversibility of the isotherm. Also, no significant changes were observed in the IR spectra, indicating that the bonds remained unchanged. This result represents, to the best of our knowledge, the first example of a Co(II)-based MOF material that demonstrates stability toward SO_2. To further this analysis, the structural stability of MUF-16 was investigated under harsher conditions involving SO_2 in the presence of water vapor (60% RH, during 24 h). Again, the PXRD pattern and IR spectra did not change (Figures S7 and S8), which demonstrates the robustness of MUF-16 and a high tolerance to SO_2 over a range of real-world conditions.

Additionally, the N_2 adsorption isotherm was measured (Figure S9), and the BET surface area was estimated, resulting in 217 m^2 g^{-1}, and by using SEM images, an average particle size of 3.06 μm (Figure S10) was determined with ImageJ software,[34] which shows that neither the porosity nor the morphology of the material is affected by harsh conditions such as SO_2 in the presence of water vapor. The above contrasts with MOFs made of Co, as for example, the material Co-URJC-5,[22] in which when exposed to SO_2, the Co(II) metal center changes in its coordination sphere from octahedral to tetrahedral, destroying the crystal structure of the material. Furthermore, it is shown that the hydrogen bonds forming the structure of MUF-16 are robust enough to prevent Co(II) from undergoing changes in its coordination sphere.

To identify the strongest SO_2 adsorption site in MUF-16, we carried out first-principles dispersion-corrected density functional (DFT-D3)[38] calculations using the VASP software package (see the Supporting Information).[39] In addition to a range of favorable electrostatic and van der Waals contacts, MUF-16 interacts with the SO_2 molecule via two hydrogen bonds (Figure 2b). In the first, the N−H functional group of the framework acts as the H-bond donor, while an O atom from the SO_2 molecule is the acceptor. The $-NH_2$···O═S═O distance is 2.523 Å. In the second, multiple −CH groups from the framework form an H-bond to the SO_2 molecule with an O···H distance varying from 2.26, to 3.1 Å. The calculated enthalpy of adsorption for the binding of this SO_2 was estimated to be −64 kJ mol^{-1}.

To gain insights into the nature of SO_2 binding in MUF-16 and its behavior, we performed grand canonical Monte Carlo (GCMC) simulations using the RASPA software package (see the Supporting Information).[40] The experimental and simulated SO_2 isotherms are in close agreement at 298 and 308 K (Figures S12 and S13), although the simulated adsorption uptake is slightly higher than the experimental data. A possible explanation is that the force field model overestimates the uptake because it is an estimate and general approach to energy distribution in the framework. Also, the presence of any defects and disorders in the synthesized sample would reduce the amount of adsorption compared to the defect-free crystal structure. A snapshot from the simulation of SO_2 in MUF-16 at 1 bar and 298 K is presented in Figure S15.

Since the DFT studies point to a strong interaction between MUF-16 and the SO_2 guest molecules, to investigate this experimentally, we carried out FT-IR spectroscopic measurements on MUF-16 and a sample that had been saturated with SO_2 (Figure 3). While most absorption bands do not shift upon SO_2 uptake, some differences are observed in the range 3350−3260 cm^{-1} (Figure 3b). Two sharp intense bands associated with the symmetric and asymmetric stretching vibrational mode of the $-NH_2$ group,[41] undergo an inversion in intensity.

Also, the classical overtone from the primary amine group at 3173 cm^{-1} disappears when MUF-16 is exposed to SO_2. In a complementary way, the band at 1681 cm^{-1}, which belongs to the N−H bending vibrational mode, develops a shoulder after SO_2 exposure (Figure 3c). According to the literature, these changes suggest that the $-NH_2$ motifs inside the channels of

https://doi.org/10.1021/acs.chemmater.3c02715
Chem. Mater. 2024, 36, 2735−2742

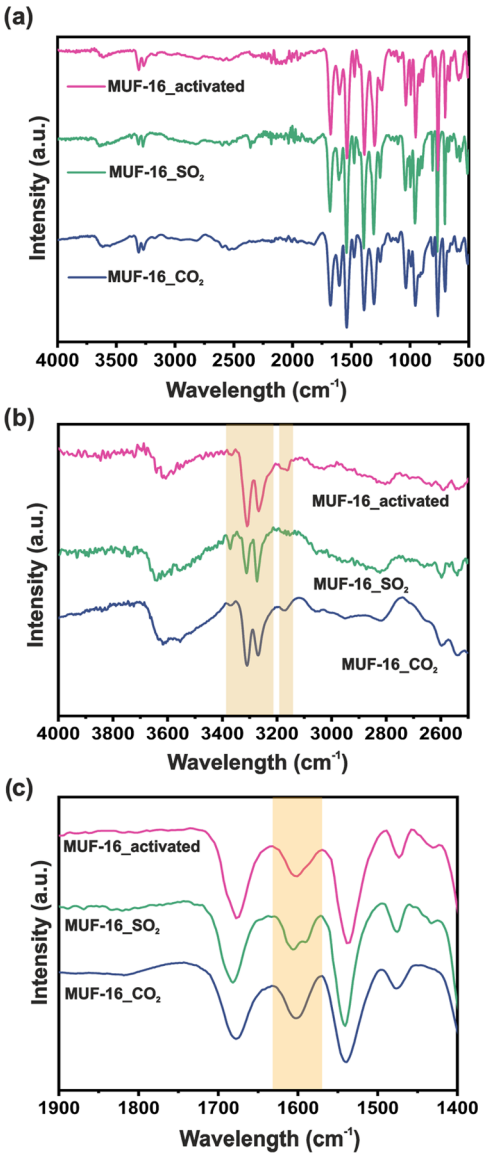

Figure 3. FT-IR spectra comparison of MUF-16 activated (pink line), saturated with SO_2 (green line), and saturated with CO_2 (blue line). (a) Complete spectrum from 4000 to 500 cm^{-1}, (b) range from 4000 to 2500 cm^{-1}, and (c) range from 1900 to 1400 cm^{-1}.

MUF-16 form hydrogen bonds, as seen in the DFT models.[42,43] In contrast to the case of SO_2, loading MUF-16 with CO_2 does not bring about significant changes.

Since SO_2 is usually present as a trace gas in gas mixtures in which CO_2 is usually a major component, we decided to investigate the SO_2 selectivity by MUF-16, using the Python package called pyIAST[44] that predicts mixed-gas adsorption isotherms in porous materials from pure-component gas adsorption isotherms using ideal adsorbed solution theory (IAST). For this purpose, a single-component CO_2 adsorption isotherm was measured (Figure S16) in which a total capture of 2.07 mmol g^{-1} at 1 bar and 298 K was obtained. Comparing this isotherm with the one obtained for SO_2, it can be observed that the total CO_2 capture is like the value obtained for SO_2 adsorption (2.22 mmol g^{-1} at 1 bar and 298 K). However, substantial differences were observed in the low-pressure range (0 to 0.2 bar), where SO_2 capture was considerably higher than the CO_2 capture, so we calculated such selectivity at that pressure range. Thus, a relatively high selectivity of 27.38 was obtained for a CO_2/SO_2:99.9/0.1 mixture and selectivity values between 24 and 27 for mixtures from CO_2/SO_2:80/20 (Table S4). This estimated selectivity can be also correlated with the reported adsorption enthalpy value for CO_2, which is −32 kJ mol^{-1}, which is a lower value than the values for SO_2 of approximately −43.7 to −51.5 kJ mol^{-1}, indicating that the interaction of SO_2 with the pore walls of MUF-16 is higher in the case of CO_2, at low coverages.

3.3. SO_2 Detection Measurements. Taking advantage of the strong SO_2 uptake at low pressure presented by MUF-16 and its high structural stability in dry and wet SO_2 conditions previously discussed, we measured the photoluminescence changes upon gas uptake. First, a UV−visible (UV−vis) spectrum was recorded to identify the wavelength range in which MUF-16 absorbs light (Figure S18), and it was found that this occurs between 300 and 400 nm. It was therefore decided to measure the emission of MUF-16 at different excitation wavelengths within its absorption wavelength range (Figure S19), and it was observed that, in all cases, the maximum emission length was 455 nm and that the emission spectrum was more intense when excited at 360 nm. To corroborate the choice of excitation wavelength of MUF-16, an excitation spectrum was performed at an emission wavelength of 455 nm, and it was found that the maximum emission was indeed at 360 nm (Figure S20). Subsequently, emission spectra of as-synthesized, activated, and saturated MUF-16 samples were performed with the following gases: SO_2, CO_2, H_2S, NO_2, N_2, O_2, CH_4, and water vapor. Since SO_2, H_2S, and NO_2 are toxic gases that were generated from hazardous and corrosive precursors (H_2SO_4, HCl, and HNO_3), it is important to emphasize that, for their generation of these gases and handling of samples exposed to these, particular safety measures were performed, such as the use of gloves, goggles, and respiratory protection. The saturations were carried out in our ex situ gas generation system (Figure S11), and prior to all saturations, MUF-16 samples were activated at 403 K under vacuum for 4 h. Figure 4a shows the MUF-16 emission spectra that were obtained for each case, showing that only for SO_2, a considerable change in fluorescence was obtained, which corroborates the good selectivity of MUF-16 for SO_2. Similar effects have been observed in other fluorescent MOFs. Recently, we conducted an experimental and theoretical investigation on the photoluminescent quenching of a copper−organic polyhedron with carbazole motifs (MOP-CDC).[30] Here, the $-NH_{carbazol}$ and oxygen atoms from the SO_2 molecule were seen to interact strongly, leading to a photoluminescence change. We propose a similar behavior for MUF-16: H-bonding between the amino groups of the framework and the SO_2 adsorbates that change the emission intensity.

To explain the low changes in fluorescence for the other molecules, we can look at their polarities and kinetic diameters. In general, the greater the electronegativity difference between the constituent atoms of a molecule and the greater the asymmetry in the geometry, the greater the polarity of the molecule. In the case of N_2 and O_2, being diatomic molecules with identical atoms, there is no polarity. For CO_2, the linear symmetry of the molecule and the similarity of electronegativities between C (3.15) and O (3.78) make it nonpolar. CH_4 is also nonpolar due to its tetrahedral symmetry and uniform charge distribution. In the above cases of nonpolar molecules, their interaction with the material is expected to be

https://doi.org/10.1021/acs.chemmater.3c02715
Chem. Mater. 2024, 36, 2735−2742

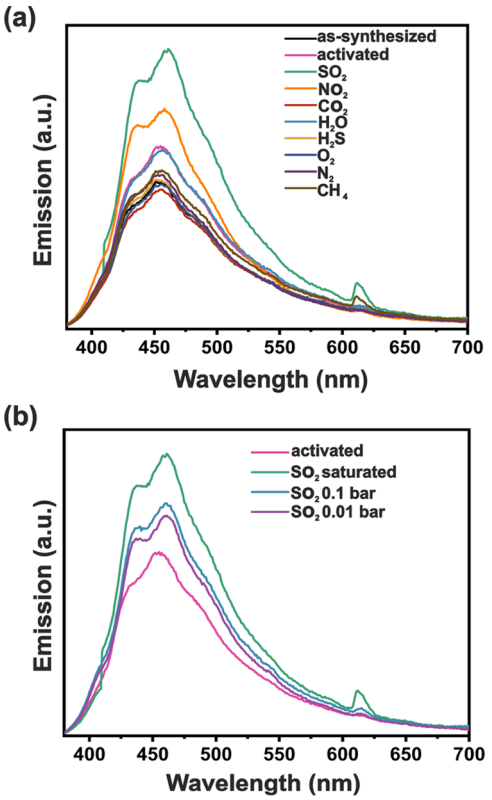

Figure 4. (a) Comparison of solid-state emission spectra of MUF-16 exposed to different gases, and (b) comparison of solid-state emission spectra of MUF-16 exposed to different SO_2 pressures.

limited or nonexistent. In contrast, H_2O, H_2S, NO_2, and SO_2 are polar molecules due to the differences in electronegativities between their atoms and their angular molecular geometries, showing dipole moments of 1.85, 0.98, 0.31, and 1.63 D, respectively.[45−47] On the other hand, the kinetic diameter is a concept used in the kinetic theory of gases to describe the interaction and collision of the molecules of a gas; in general terms, a larger kinetic diameter suggests a higher probability of collision in the hard-sphere model. The kinetic diameter values are 2.65, 3.60, 3.30, and 4.10 Å for H_2O, H_2S, NO_2, and SO_2, respectively.[48,49] Considering that SO_2 is a highly polar molecule compared to its competitors and shows the largest kinetic diameter among the tested molecules, it is understandable why MUF-16 can form more specific interactions with this gas, leading to changes in fluorescence, while the other molecules, displaying lower dipole moments, are less likely to interact with the material and therefore do not induce significant changes in fluorescence.

To elucidate a possible fluorescence mechanism causing the observed emission change, time-resolved photoluminescence (TRPL) experiments were performed (Figure S21), and quantum yields were measured for activated and SO_2-saturated MUF-16 samples. The fluorescence lifetime for the activated sample was found to be 1.71 ns, while the one for the saturated sample was equal to 2.29 ns. The quantum yields were 0.63 and 7.89%, respectively, for the activated and saturated samples. These results show that the presence of SO_2 changes the fluorescence lifetime of MUF-16 and increases the efficiency for the material to convert the absorbed energy into light, indicating that the presence of SO_2 favors radiative dissipation mechanisms (with duration in the order of 10^{-9} s) over nonradiative ones (with duration in the order of 10^{-12} s),[50] which increases of the fluorescence lifetime. In this work, we propose that the presence of SO_2, which establishes hydrogen bonds with MUF-16, induces a rigidification in the framework of the material, generating changes in the electronic structure of the system and disfavoring the nonradiative dissipation pathways such as vibrational relaxation.

In addition, we tested the fluorescence of samples exposed to 0.1 and 0.01 bar, observing that in both cases, MUF-16 shows a fluorescence response (Figure 4b). The effect that water vapor and CO_2 can potentially have on the response of the fluorescence for the material when evaluating SO_2, was also evaluated. For this purpose, independent MUF-16 samples were exposed to 0.1 bar of SO_2 in the ex situ gas generation system, and simultaneously, approximately 0.9 bar of water vapor and CO_2 were introduced into the system, and their emission spectra were measured. It was found that there were no significant changes in the intensity or shape of the fluorescence spectra with respect to the spectrum of the sample exposed to only 0.1 bar (Figure S22). On the other hand, to test the durability of the material as a detector, five cycles of reactivation and saturation with SO_2 were performed on the same sample of MUF-16, showing that, in all cases, the intensity of the material changes in the same way (Figure S23), demonstrating that MUF-16 is a recyclable material in the context of the fluorescent detection of SO_2.

To further analyze MUF-16 for the detection of SO_2, the limit of detection (LOD) was calculated using a solution of SO_2 dissolved in THF. The LOD value was calculated with the following formula: LOD = $3\sigma/m$, where σ represents the standard deviation of the initial intensity of pristine MUF-16 in THF and m is the slope of the linear fit from the experimental data. Different solutions were measured in the range 1−250 mM (Figures S24 and S25). In this case, the LOD was calculated to be 1.26 mM (~80.72 ppm) of SO_2 in a THF solution.

4. CONCLUSIONS

To summarize, we report the reversible experimental SO_2 adsorption−desorption for MUF-16 with a total SO_2 uptake of 2.2 mmol g^{-1} and a highly competitive SO_2 uptake of 2.1 mmol g^{-1} at only 0.1 bar. This relatively high SO_2 adsorption at low pressure (~0.1 bar) suggests that the material exhibits a preferential adsorption domain. To elucidate the SO_2 adsorption mechanism, FT-IR experiments were performed, observing that once an MUF-16 sample is saturated with SO_2, the bands related to the $-NH_2$ group clearly change, corroborating an SO_2-NH_2 interaction. Complementary, this material shows selective detection of SO_2 since the effect of the SO_2 molecule quenched its emission. These experimental results were supported by DFT calculations that indicated that the SO_2 molecule is located in the vicinity of the NH_2 functional group. In addition, MUF-16 displays a high change in its fluorescence performances for SO_2 compared to other gases (SO_2, CO_2, NO_2, N_2, O_2, CH_4, and water vapor), demonstrating its high affinity for a possible detection application of SO_2. The possible florescence mechanism was determined using time-resolved photoluminescence. Finally, the LOD was calculated to be 1.26 mM (~80.72 ppm) of SO_2 in a THF solution.

https://doi.org/10.1021/acs.chemmater.3c02715
Chem. Mater. 2024, 36, 2735−2742

■ ASSOCIATED CONTENT

Supporting Information

The Supporting Information is available free of charge at https://pubs.acs.org/doi/10.1021/acs.chemmater.3c02715.

Experimental details; PXRD patterns after SO_2 exposure; isosteric heat of adsorption of SO_2, SO_2 adsorption−desorption cycles, and SO_2 testing in humid conditions; computational studies; and fluorescence details (PDF)

■ AUTHOR INFORMATION

Corresponding Authors

Diego Solís-Ibarra − *Laboratorio de Fisicoquímica y Reactividad de Superficies (LaFReS), Instituto de Investigaciones en Materiales, Universidad Nacional Autónoma de México, 04510 México D.F., México;* orcid.org/0000-0002-2486-0967; Email: diego.solis@unam.mx

Ilich A. Ibarra − *Laboratorio de Fisicoquímica y Reactividad de Superficies (LaFReS), Instituto de Investigaciones en Materiales, Universidad Nacional Autónoma de México, 04510 México D.F., México; On sabbatical as "Catedra Dr. Douglas Hugh Everett" at Departamento de Química, Universidad Autónoma Metropolitana-Iztapalapa, 09310 Ciudad de México, México;* orcid.org/0000-0002-8573-8033; Email: argel@unam.mx

Shane G. Telfer − *MacDiarmid Institute for Advanced Materials and Nanotechnology, School of Natural Sciences, Massey University, Palmerston North 4410, New Zealand;* orcid.org/0000-0003-1596-6652; Email: S.Telfer@massey.ac.nz

Authors

Valeria B. López-Cervantes − *Laboratorio de Fisicoquímica y Reactividad de Superficies (LaFReS), Instituto de Investigaciones en Materiales, Universidad Nacional Autónoma de México, 04510 México D.F., México*

Alfredo López-Olvera − *Laboratorio de Fisicoquímica y Reactividad de Superficies (LaFReS), Instituto de Investigaciones en Materiales, Universidad Nacional Autónoma de México, 04510 México D.F., México*

Juan L. Obeso − *Laboratorio de Fisicoquímica y Reactividad de Superficies (LaFReS), Instituto de Investigaciones en Materiales, Universidad Nacional Autónoma de México, 04510 México D.F., México; Instituto Politécnico Nacional, CICATA U. Legaria, Laboratorio Nacional de Ciencia, Tecnología y Gestión Integrada del Agua (LNAgua), 11500 Ciudad de México, México*

Iván Kaleb Torres − *Laboratorio de Fisicoquímica y Reactividad de Superficies (LaFReS), Instituto de Investigaciones en Materiales, Universidad Nacional Autónoma de México, 04510 México D.F., México*

Eva Martínez-Ahumada − *Laboratorio de Fisicoquímica y Reactividad de Superficies (LaFReS), Instituto de Investigaciones en Materiales, Universidad Nacional Autónoma de México, 04510 México D.F., México*

Paulina Carmona-Monroy − *Laboratorio de Fisicoquímica y Reactividad de Superficies (LaFReS), Instituto de Investigaciones en Materiales, Universidad Nacional Autónoma de México, 04510 México D.F., México*

Elí Sánchez-González − *Laboratorio de Fisicoquímica y Reactividad de Superficies (LaFReS), Instituto de Investigaciones en Materiales, Universidad Nacional Autónoma de México, 04510 México D.F., México*

Enrique Lima − *Laboratorio de Fisicoquímica y Reactividad de Superficies (LaFReS), Instituto de Investigaciones en Materiales, Universidad Nacional Autónoma de México, 04510 México D.F., México*

Elnaz Jangodaz − *MacDiarmid Institute for Advanced Materials and Nanotechnology, School of Natural Sciences, Massey University, Palmerston North 4410, New Zealand;* orcid.org/0000-0003-4902-3273

Ravichandar Babarao − *School of Science, RMIT University, Centre for Advanced Materials and Industrial Chemistry, Melbourne, Victoria 3001, Australia;* orcid.org/0000-0003-3556-495X

Complete contact information is available at: https://pubs.acs.org/10.1021/acs.chemmater.3c02715

Author Contributions

#V.B.L.-C., A.L.-O., and J.L.O. contributed equally to this work.

Notes

The authors declare no competing financial interest.

■ ACKNOWLEDGMENTS

V.B.L.-C. and J.L.O. thank CONAHCYT for the Ph.D. fellowship (1005649 and 1003953). I.A.I. thanks PAPIIT UNAM (IN201123), México, for financial support. The authors thank U. Winnberg (Euro Health) for scientific discussions and G. Ibarra-Winnberg for scientific encouragement. R.B acknowledges the National Computing Infrastructure for providing the computational resources.

■ REFERENCES

(1) Fuller, R.; Landrigan, P. J.; Balakrishnan, K.; Bathan, G.; Bose-O'Reilly, S.; Brauer, M.; Caravanos, J.; Chiles, T.; Cohen, A.; Corra, L.; Cropper, M.; Ferraro, G.; Hanna, J.; Hanrahan, D.; Hu, H.; Hunter, D.; Janata, G.; Kupka, R.; Lanphear, B.; Lichtveld, M.; Martin, K.; Mustapha, A.; Sanchez-Triana, E.; Sandilya, K.; Schaefli, L.; Shaw, J.; Seddon, J.; Suk, W.; Téllez-Rojo, M. M.; Yan, C. Pollution and Health: A Progress Update. *Lancet Planet. Health* **2022**, *6* (6), e535−e547.

(2) del C Cotlame-Salinas, V.; López-Olvera, A.; Islas-Jácome, A.; González-Zamora, E.; Ibarra, I. A. CO_2 Capture Enhancement in MOFs via the Confinement of Molecules. *React. Chem. Eng.* **2021**, *6* (3), 441−453.

(3) Schwartz, J.; Dockery, D. W. Increased Mortality in Philadelphia Associated with Daily Air Pollution Concentrations. *Am. Rev. Respir. Dis.* **1992**, *145* (3), 600−604.

(4) Amoatey, P.; Omidvarborna, H.; Baawain, M. S.; Al-Mamun, A. Emissions and Exposure Assessments of SO_X, NO_X, $PM_{10/2.5}$ and Trace Metals from Oil Industries: A Review Study (2000−2018). *Process Saf. Environ. Prot.* **2019**, *123*, 215−228.

(5) Qian, Y.; Behrens, P.; Tukker, A.; Rodrigues, J. F. D.; Li, P.; Scherer, L. Environmental Responsibility for Sulfur Dioxide Emissions and Associated Biodiversity Loss across Chinese Provinces. *Environ. Pollut.* **2019**, *245*, 898−908.

(6) Hansell, A.; Oppenheimer, C. Health Hazards from Volcanic Gases: A Systematic Literature Review. *Arch. Environ. Health Int. J.* **2004**, *59* (12), 628−639.

(7) Wei, H.; Liu, W.; Zhang, J.; Qin, Z. Effects of Simulated Acid Rain on Soil Fauna Community Composition and Their Ecological Niches. *Environ. Pollut.* **2017**, *220*, 460−468.

(8) Kitadai, N.; Maruyama, S. Origins of Building Blocks of Life: A Review. *Geosci. Front.* **2018**, *9* (4), 1117−1153.

(9) Dales, R.; Chen, L.; Frescura, A. M.; Liu, L.; Villeneuve, P. J. Acute Effects of Outdoor Air Pollution on Forced Expiratory Volume in 1 s: A Panel Study of Schoolchildren with Asthma. *Eur. Respir. J.* **2009**, *34* (2), 316−323.
(10) Orellano, P.; Reynoso, J.; Quaranta, N. Short-Term Exposure to Sulphur Dioxide (SO_2) and All-Cause and Respiratory Mortality: A Systematic Review and Meta-Analysis. *Environ. Int.* **2021**, *150*, No. 106434.
(11) Sotirchos, S. V.; Smith, A. R. Performance of Porous CaO Obtained from the Decomposition of Calcium-Enriched Bio-Oil as Sorbent for SO_2 and H_2S Removal. *Ind. Eng. Chem. Res.* **2004**, *43* (6), 1340−1348.
(12) Ortiz, F. J. G.; Vidal, F.; Ollero, P.; Salvador, L.; Cortés, V.; Giménez, A. Pilot-Plant Technical Assessment of Wet Flue Gas Desulfurization Using Limestone. *Ind. Eng. Chem. Res.* **2006**, *45* (4), 1466−1477.
(13) Zhang, L.; Xiao, L.; Zhang, Y.; France, L. J.; Yu, Y.; Long, J.; Guo, D.; Li, X. Synthesis of Ionic Liquid-SBA-15 Composite Materials and Their Application for SO_2 Capture from Flue Gas. *Energy Fuels* **2018**, *32* (1), 678−687.
(14) Westmoreland, P. R.; Harrison, D. P. Evaluation of Candidate Solids for High-Temperature Desulfurization of Low-Btu Gases. *Environ. Sci. Technol.* **1976**, *10* (7), 659−661.
(15) Li, B.; Ma, C. Study on the Mechanism of SO2 Removal by Activated Carbon. *Energy Procedia* **2018**, *153*, 471−477.
(16) Pérez-Botella, E.; Valencia, S.; Rey, F. Zeolites in Adsorption Processes: State of the Art and Future Prospects. *Chem. Rev.* **2022**, *122* (24), 17647−17695.
(17) Yumura, M.; Furimsky, E. Comparison of Calcium Oxide, Zinc Oxide, and Iron(III) Oxide Hydrogen Sulfide Adsorbents at High Temperatures. *Ind. Eng. Chem. Process Des. Dev.* **1985**, *24* (4), 1165−1168.
(18) Zhou, H.-C.; Long, J. R.; Yaghi, O. M. Introduction to Metal−Organic Frameworks. *Chem. Rev.* **2012**, *112* (2), 673−674.
(19) López-Cervantes, V. B.; Obeso, J. L.; Yañez-Aulestia, A.; Islas-Jácome, A.; Leyva, C.; González-Zamora, E.; Sánchez-González, E.; Ibarra, I. A. MFM-300(Sc): A Chemically Stable Sc(III)-Based MOF Material for Multiple Applications. *Chem. Commun.* **2023**, *59* (69), 10343−10359.
(20) Martínez-Ahumada, E.; Díaz-Ramírez, M. L.; Lara-García, H. A.; Williams, D. R.; Martis, V.; Jancik, V.; Lima, E.; Ibarra, I. A. High and Reversible SO_2 Capture by a Chemically Stable Cr(III)-Based MOF. *J. Mater. Chem. A* **2020**, *8* (23), 11515−11520.
(21) Martínez-Ahumada, E.; Kim, D. w.; Wahiduzzaman, M.; Carmona-Monroy, P.; López-Olvera, A.; Williams, D. R.; Martis, V.; Lara-García, H. A.; López-Morales, S.; Solis-Ibarra, D.; Maurin, G.; Ibarra, I. A.; Hong, C. S. Capture and Detection of SO_2 Using a Chemically Stable Mg(II)−MOF. *J. Mater. Chem. A* **2022**, *10* (36), 18636−18643.
(22) López-Olvera, A.; Montes-Andrés, H.; Martínez-Ahumada, E.; López-Cervantes, V. B.; Martínez-Serrano, R. D.; González-Zamora, E.; Martínez, A.; Leo, P.; Martos, C.; Ibarra, I. A.; Orcajo, G. Understanding the Mechanism of Amorphization for Co-URJC-5. *Eur. J. Inorg. Chem.* **2021**, *2021* (43), 4458−4462.
(23) Nazari, S.; Shahhoseini, O.; Sohrabi-Kashani, A.; Davari, S.; Paydar, R.; Delavar-Moghadam, Z. Experimental Determination and Analysis of CO_2, SO_2 and NO_x Emission Factors in Iran's Thermal Power Plants. *Energy* **2010**, *35* (7), 2992−2998.
(24) Speidel, M.; Nau, R.; Arnold, F.; Schlager, H.; Stohl, A. Sulfur Dioxide Measurements in the Lower, Middle and Upper Troposphere: Deployment of an Aircraft-Based Chemical Ionization Mass Spectrometer with Permanent in-Flight Calibration. *Atmos. Environ.* **2007**, *41* (11), 2427−2437.
(25) Cheng, Y.; Wang, S.; Zhu, J.; Guo, Y.; Zhang, R.; Liu, Y.; Zhang, Y.; Yu, Q.; Ma, W.; Zhou, B. Surveillance of SO_2 and NO_2 from Ship Emissions by MAX-DOAS Measurements and the Implications Regarding Fuel Sulfur Content Compliance. *Atmos. Chem. Phys.* **2019**, *19* (21), 13611−13626.
(26) Okabe, H.; Splitstone, P. L.; Ball, J. J. Ambient and Source SO_2 Detector Based on a Fluorescence Method. *J. Air Pollut. Control Assoc.* **1973**, *23* (6), 514−516.
(27) Chernikova, V.; Yassine, O.; Shekhah, O.; Eddaoudi, M.; Salama, K. N. Highly Sensitive and Selective SO_2 MOF Sensor: The Integration of MFM-300 MOF as a Sensitive Layer on a Capacitive Interdigitated Electrode. *J. Mater. Chem. A* **2018**, *6* (14), 5550−5554.
(28) Tchalala, M. R.; Bhatt, P. M.; Chappanda, K. N.; Tavares, S. R.; Adil, K.; Belmabkhout, Y.; Shkurenko, A.; Cadiau, A.; Heymans, N.; De Weireld, G.; Maurin, G.; Salama, K. N.; Eddaoudi, M. Fluorinated MOF Platform for Selective Removal and Sensing of SO_2 from Flue Gas and Air. *Nat. Commun.* **2019**, *10* (1), No. 1328.
(29) Wang, M.; Guo, L.; Cao, D. Amino-Functionalized Luminescent Metal−Organic Framework Test Paper for Rapid and Selective Sensing of SO_2 Gas and Its Derivatives by Luminescence Turn-On Effect. *Anal. Chem.* **2018**, *90* (5), 3608−3614.
(30) Martínez-Ahumada, E.; López-Olvera, A.; Carmona-Monroy, P.; Díaz-Salazar, H.; Garduño-Castro, M. H.; Obeso, J. L.; Leyva, C.; Martínez, A.; Hernández-Rodríguez, M.; Solis-Ibarra, D.; Ibarra, I. A. SO_2 Capture and Detection Using a Cu(II)-Metal−Organic Polyhedron. *Dalton Trans.* **2022**, *51* (48), 18368−18372.
(31) Qazvini, O. T.; Telfer, S. G. MUF-16: A Robust Metal−Organic Framework for Pre- and Post-Combustion Carbon Dioxide Capture. *ACS Appl. Mater. Interfaces* **2021**, *13* (10), 12141−12148.
(32) Sathya Priyadarshini, G.; Selvi, G. Luminescence Cobalt(II) Complexes: Synthesis, Characterization, Photophysical and DFT Study. *Mater. Today Proc.* **2021**, *40*, S19−S27.
(33) Qazvini, O. T.; Babarao, R.; Telfer, S. G. Selective Capture of Carbon Dioxide from Hydrocarbons Using a Metal-Organic Framework. *Nat. Commun.* **2021**, *12* (1), No. 197.
(34) Collins, T. J. ImageJ for Microscopy. *Biotechniques* **2007**, *43* (1S), S25−S30.
(35) López-Cervantes, V. B.; Bara, D.; Yañez-Aulestia, A.; Martínez-Ahumada, E.; López-Olvera, A.; Amador-Sánchez, Y. A.; Solis-Ibarra, D.; Sánchez-González, E.; Ibarra, I. A.; Forgan, R. S. Modulated Self-Assembly of Three Flexible Cr(III) PCPs for SO_2 Adsorption and Detection. *Chem. Commun.* **2023**, *59* (52), 8115−8118.
(36) Domínguez-González, R.; Rojas-León, I.; Martínez-Ahumada, E.; Martínez-Otero, D.; Lara-García, H. A.; Balmaseda-Era, J.; Ibarra, I. A.; Percástegui, E. G.; Jancik, V. UNAM-1: A Robust Cu I and Cu II Containing 3D-Hydrogen-Bonded Framework with Permanent Porosity and Reversible SO_2 Sorption. *J. Mater. Chem. A* **2019**, *7* (47), 26812−26817.
(37) Nuhnen, A.; Janiak, C. A Practical Guide to Calculate the Isosteric Heat/Enthalpy of Adsorption via Adsorption Isotherms in Metal−Organic Frameworks, MOFs. *Dalton Trans.* **2020**, *49* (30), 10295−10307.
(38) Grimme, S.; Ehrlich, S.; Goerigk, L. Effect of the Damping Function in Dispersion Corrected Density Functional Theory. *J. Comput. Chem.* **2011**, *32* (7), 1456−1465.
(39) Kresse, G.; Hafner, J. Ab Initio Molecular Dynamics for Open-Shell Transition Metals. *Phys. Rev. B* **1993**, *48* (17), 13115−13118.
(40) Dubbeldam, D.; Calero, S.; Ellis, D. E.; Snurr, R. Q. RASPA: Molecular Simulation Software for Adsorption and Diffusion in Flexible Nanoporous Materials. *Mol. Simul.* **2016**, *42* (2), 81−101.
(41) Hadjiivanov, K. I.; Panayotov, D. A.; Mihaylov, M. Y.; Ivanova, E. Z.; Chakarova, K. K.; Andonova, S. M.; Drenchev, N. L. Power of Infrared and Raman Spectroscopies to Characterize Metal-Organic Frameworks and Investigate Their Interaction with Guest Molecules. *Chem. Rev.* **2021**, *121* (3), 1286−1424.
(42) Lady, J. H.; Whetsel, K. B. Infrared Studies of Amine Complexes. IV. The N-H-O Hydrogen Bond in Aromatic Amine Complexes of Ethers Ketones, Esters, and Amides. *J. Phys. Chem. A* **1967**, *71* (5), 1421−1429.
(43) Ryu, I. S.; Liu, X.; Jin, Y.; Sun, J.; Lee, Y. J. Stoichiometric Analysis of Competing Intermolecular Hydrogen Bonds Using Infrared Spectroscopy. *RSC Adv.* **2018**, *8* (42), 23481−23488.

https://doi.org/10.1021/acs.chemmater.3c02715
Chem. Mater. 2024, 36, 2735−2742

(44) Simon, C. M.; Smit, B.; Haranczyk, M. PyIAST: Ideal Adsorbed Solution Theory (IAST) Python Package. *Comput. Phys. Commun.* **2016**, *200*, 364−380.
(45) Azzam, A. A. A.; Lodi, L.; Yurchenko, S. N.; Tennyson, J. The Dipole Moment Surface for Hydrogen Sulfide H_2S. *J. Quant. Spectrosc. Radiat. Transfer* **2015**, *161*, 41−49.
(46) Shostak, S. L.; Ebenstein, W. L.; Muenter, J. S. The Dipole Moment of Water. I. Dipole Moments and Hyperfine Properties of H_2O and HDO in the Ground and Excited Vibrational States. *J. Chem. Phys.* **1991**, *94* (9), 5875−5882.
(47) Hodgeson, J. A.; Sibert, E. E.; Curl, R. F. DIPOLE MOMENT OF NITROGEN DIOXIDE 1a. *J. Phys. Chem. A* **1963**, *67* (12), 2833−2835.
(48) Kentish, S.; Scholes, C.; Stevens, G. Carbon Dioxide Separation through Polymeric Membrane Systems for Flue Gas Applications. *Recent Patents Chem. Eng.* **2008**, *1* (1), 52−66.
(49) Seehamart, K.; Busayaporn, W.; Chanajaree, R.Excitation Energy Transfer. In *Molecular Fluorescence: Principles and Applications*, 2nd ed.; Wiley, 2023.
(50) Valeur, B.; Berberan-Santos, N. Excitation Energy Transfer. In *Molecular Fluorescence: Principles and Applications*; Wiley, 2012.

https://doi.org/10.1021/acs.chemmater.3c02715
Chem. Mater. 2024, 36, 2735−2742